Embrittlement of Nuclear Reactor Pressure Vessels

G.R. Odette and G.E. Lucas

Editor's Note: A hypertext-enhanced version of this article can be found at www.tms.org/pubs/journals/JOM/0107/Odette-0107.html

Neutron irradiation embrittlement could limit the service life of some of the reactor-pressure vessels in existing commercial nuclear-power plants. Improved understanding the of the underlying causes of embrittlement has provided regulators and power-plant operators better estimates of vessel-operating margins. This article presents an overview of embrittlement, emphasizing the status of mechanistic understanding and models, and their role in increasing the reliability of vessel-integrity assessments. Finally, a number of outstanding issues and significant opportunities, including a new fracture-toughness master-curve method, are briefly described.

INTRODUCTION

Light water reactors generate a large majority of the world's nuclear energy. Achieving reasonable thermodynamic efficiency requires a heavy-section steel reactor pressure vessel (RPV) to safely contain coolant water at temperatures around 290°C at pressures ranging from ≈7 MPa in boiling water reactors (BWR) to ≈14 MPa in pressurized water reactors (PWR). Regulations require very low RPV failure probabilities both for normal operation and postulated accident events.[1–3] Vessel designs and integrity assessment assume the presence of large cracks and rare, but severe, loading conditions, such as pressurized thermal shock. This combination could conceivably result in catastrophic fast fracture if the vessel steel is sufficiently brittle.

Vessel-integrity assessments require activities ranging from in-service flaw inspections to system-scale thermal-hydraulic stress analysis. However, a basic safety criterion is that the RPV steels remain sufficiently tough. The toughness of a material can be measured in a variety of ways. RPV integrity assessments require evaluations of sharp crack, mode I fracture toughness-temperature curves for static $K_{Jc}[T]$, dynamic $K_{Id}[T]$ and arrest $K_{Ia}[T]$ loading conditions in the cleavage transition regime, as well J-R based measures of ductile initiation and tearing resistance toughness. This article focuses on issues related to the cleavage transition regime but, due to length limits, will not try to distinguish between the various types of $K_I(T)$. Toughness is not an issue for as-fabricated vessels. However, exposure to neutrons in the so-called beltline region of the vessel surrounding the reactor core degrades the fracture toughness of RPV steels. Irradiation embrittlement is usually characterized by the increase in a ductile-to-brittle transition temperature (DBTT) that marks the transition between low toughness brittle (cleavage) and high toughness ductile (microvoid coalescence) fracture regimes. Transition temperature shifts have exceeded 200°C in some cases.[4] Hence, embrittlement must be considered in RPV integrity[3] assessments and, if severe, may require either premature plant closure or vessel annealing.

Improvements over recent decades that have reduced the problem of RPV embrittlement include tougher steels with lower trace impurity contents, reductions in the neutron flux impinging on the vessel, and elimination of beltline welds. However, embrittlement remains a potential issue for some older vessels, and is an unknown for the extended life of others.

VESSELS, STEELS AND SERVICE ENVIRONMENTS

U.S. RPV technology is reasonably representative of the approaches used worldwide. RPVs are massive welded structures, weighing up to 500 tonnes, standing 14 m high by 4.5 m in diameter with a wall thickness up to 20 cm or more. Typical RPV base metals are A302B, A533B plates, or A508 forgings, which are quenched and tempered, low-alloy steels with primarily tempered bainitic microstructures. Typical compositions are C(0.05–0.2%), Mn(0.7–1.6%), Mo(0.4–0.6%), Ni(0.2–1.4%), Si(0.2–0.6%), and Cr (0.05–0.5%). Multiple-layer submerged arc welds, made of consumable metal wires, join vessel sections. Weld compositions differ from the base metal, and may vary significantly even within the same weld. Following welding, vessels are tempered and stress relieved, typically at about 620±15°C for about 30 h, resulting in as-fabricated yield stress values of about 475±50 MPa. Compositions and microstructures vary on both the macro- and micro-scales. Along with nickel alloying additions, trace impurity copper and phosphorous increase embrittlement. Copper contents are quite high (up to 0.4%) in some early U.S. welds.

Vessels operate at temperatures (T_i) of about 290±30°C and are exposed to a spectrum of neutron energies ranging from less than one to several million electron volts (MeV). High-energy neutrons are the dominant source of embrittlement. The neutron flux (ϕ) is defined as the number of neutrons crossing a unit area per unit time (neutrons/m^2-s) and the neutron fluence (ϕt) is the flux integrated over time (neutrons/m^2). A standard unit of neutron exposure is the ϕt greater than 1 MeV ($\phi t_{>1}$). The end-of-life $\phi t_{>1}$ for U.S. PWRs is about $1–3 \times 10^{23}$ n/m^2, and about an order of magnitude lower in BWRs.

MEASURES OF IRRADIATION EMBRITTLEMENT

Early recognition of the importance of embrittlement by regulators and the nuclear industry led to RPV surveillance programs. Many reactors include capsules containing representative steels that are located on the inside of the RPV where the ϕ is several times higher than in the vessel itself. Thus, the surveillance data are used to provide early estimates of the embrittlement of a given vessel, and collectively represent a database for assessing and predicting embrittlement. Numerous accelerated test-reactor studies of embrittlement have also been conducted.

Measurements of fracture toughness (e.g., K_{Ic}) require special specimens and relatively sophisticated test procedures that were not available at the time surveillance programs were first implemented. Thus, small 10 × 10 × 55 mm Charpy-V-notch (CVN) impact specimens are typically used in surveillance programs. The Charpy impact energy-temperature curve is used to determine a DBTT (T_t), indexed at an absorbed energy of 41 Joules. Neutron irradiation elevates T_t (ΔT_t) and decreases the CVN upper-shelf energy. The ΔT_t is used to shift an unirradiated ASME lower-bound reference toughness-temperature curve, $K_{Ir}(T - T_{ndt})$. The T_{ndt} is the so-called the nil-ductility transition temperature for the unirradiated steel, which is determined using a rather complex procedure, generally based on either Charpy or drop weight tests. In irradiated steel, the $K_{Ir}(T - T_{ndt} - \Delta T_t)$ curve is shifted up in temperature by the ΔT_t, which includes a margin term. While showing a great deal of early foresight, this procedure is somewhat arcane and often lacks a rigorous physical justification, particularly for steels with low upper-shelf energy. Recently, a potentially far superior master curve (MC) method for directly establishing irradiated toughness-temperature curves has been proposed.[5] The MC method is briefly described below.

Plant-specific surveillance data are usually not sufficient to predict ΔT_t. More commonly, the ΔT_t are evaluated using regulatory equations based on a large collection of surveillance data from many plants.[3,4] The ΔT_t is controlled by many variables. Recent, physically based, statistical fits to the U.S. surveillance database show that the ΔT_t depends on T_i, ϕ, $\phi t_{>1}$, Cu, Ni, P, and product form (weld, plate, and forging).[4] Single-variable, test reactor studies show that ΔT_t also depends on a number of other variables including manganese content and final heat-treatment conditions.[6] Predictive models must also account for strong synergistic interactions between variables, such as copper nickel.

Post-irradiation annealing (PIA) at temperatures (T_a) well above T_i results in partial to nearly full embrittlement recovery, depending on the Cu, T_i, T_a, ϕ, and annealing time (t_i).[7] The rate of re-irradiation embrittlement following annealing is an important issue, but it is not yet fully characterized.

Because of the number of variables and variable combinations (e.g., Cu-Ni-ϕ-ϕt-T_i, T_a, t_a), coupled with various limitations in the surveillance and PIA databases, purely empirical ΔT_t predictions are unreliable, particularly when extrapolated to conditions beyond the existing variable range (e.g., higher ϕt). Fortunately, basic mechanistic research has provided much improved understanding and physically based models of embrittlement that have improved statistical data correlations.[4,6]

EMBRITTLEMENT MECHANISMS AND MODELS

The primary mechanism of embrittlement is the hardening produced by nanometer features that develop as a consequence of irradiation. The key embrittlement processes, illustrated in Figure 1, include:[6]

- Generation of lattice defects in displacement cascades by high-energy recoil atoms from neutron scattering and reactions. The primary defects are in the form of single and small clusters of vacancies and self-interstitials (Figure 1a).
- Diffusion of primary defects also leading to enhanced solute diffusion and formation of nanoscale defect-solute cluster complexes, solute clusters, and distinct phases, primarily copper-rich precipitates (CRPs) (Figure 1b).
- Dislocation pinning and hardening by these nanofeatures (Figure 1c).
- Hardening-induced ΔT_t shifts (Figure 1d and e).

Submodels of these processes can be combined to model ΔT_t as a function of the key metallurgical (Cu, Ni, P . . .), and irradiation (ϕ, $\phi t_{>1}$, Ti . . .) variables.[4,6,8,9]

Hardening and Hardening-Induced DBTT Shifts

Cleavage occurs at a sufficiently high yield stress (σ_y) when a notch or crack tip stress concentration exceeds a critical stress (σ^*) over a microstructurally significant length scale, λ^*. Stresses ahead of a loaded notch or crack have peak values that are a small multiple (M~2–5) of σ_y. Since σ_y increases with decreasing temperature, a ductile-to-brittle transition occurs below a T* at which $M\sigma_y(T^*) = \sigma^*$ over λ^*. Irradiation induced P segregation to grain boundaries may decrease σ^*, and hence, elevate DBTT. However, the primary cause of embrittlement in western RPV steels is irradiation hardening. Specifically, increases in yield stress ($\Delta\sigma_y$) raise the temperature at which $M[\sigma_{yu}(T) + \Delta\sigma_y] = \sigma^*$, where $\sigma_{yu}(T)$ is the unirradiated yield stress. Detailed micromechanical models are consistent with observed empirical relations between $\Delta\sigma_y$ and the CVN ΔT_t, as $\Delta T_t \approx [0.6\pm0.2°C/MPa]\Delta\sigma_y$.[10]

Increases in σ_y induced by irradiation arise from the evolution of very fine nm-scale features. The individual contribution of a particular nanofeature is given by $\sigma_{yj} \approx M\alpha_j(d_j)Gb\sqrt{N_j d_j}$, where M is the Taylor factor, G is the shear modulus, b is the Burgers vector, and N_j and d_j are the number density and diameter of the feature, respectively. The $\alpha_j(d_j)$ is a strength factor that depends on the details of the dislocation-obstacle interaction process, hence, the size and characteristics of the feature. For irradiation-induced nanofeatures, dislocation pinning is generally weak and $\alpha_j(d_j)$ is < 0.4. An additional complication is that the net $\Delta\sigma_y$ is not a simple linear or root square sum of the contributions of the individual features. This arises from the fact that the individual σ_{yj} are superimposed on each other and with pre-existing strong obstacle strengthening in a way that is controlled by the shape of the stressed dislocation lines, hence, the overall combination of obstacle strength. The strong obstacles are largely fine-scale Mo_2C carbides that provide considerable strengthening in the unirradiated steel that are unaltered by irradiation. A combination of experiments and computer simulations have been used to evaluate both $\alpha_j(d_j)$ and to establish superposition relations for typical irradiation-induced features.[6]

Primary Defect Production

Current understanding of primary damage production is largely based on molecular dynamics[11] and Monte Carlo computer simulations,[12] as well as indirect experimental measurements. Neutrons create vacancies and self-interstitials (SI), separated by some distance, by displacing atoms from their normal crystal lattice sites. The displacements are produced in cascades resulting from highly energetic primary recoiling atoms (PRA) generated by neutron scattering and reactions. The interaction of a high-energy neutron with an atomic nucleus results in significant energy transfer (R). For example, a 1 MeV neutron transfers up to about 70 keV to an iron PRA (Figure 2a). Some recoil energy is lost to electrons, resulting in a somewhat lower kinetic energy that is dissipated in atomic collisions, R_d < R. The PRA kinetic energy is quickly transferred by secondary, tertiary, and n-subsequent generations of collision displacements, producing 2^n recoiling atoms at lower energies ($\approx R_d/2^n$). The process terminates when the kinetic energy of the nth-generation of recoils falls below that needed to cause additional displacements (Figure 2b). On average, a PRA creates $\nu \approx R_d/2D$ displacements, where

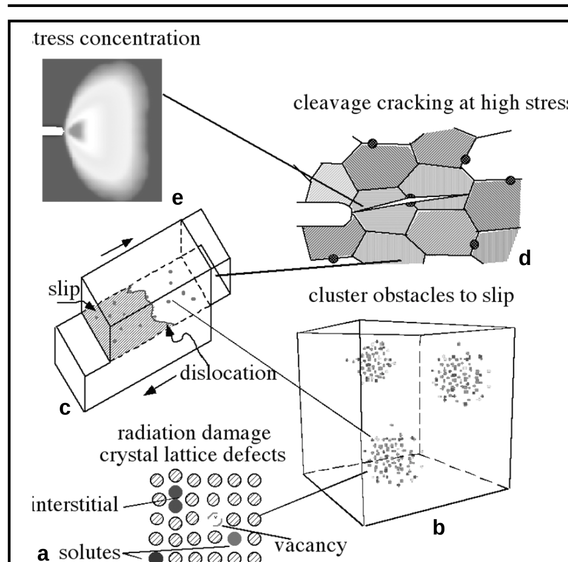

Figure 1. An illustration of the sequence of basic embrittlement processes: (a) creation of primary radiation damage defects: (b) formation of nanoscale solute and defect clusters (iron atoms not shown); (c) pinning of dislocations and hardening by nanofeatures; (d) hardening enhanced cleavage fracture; at a (e) stress concentration.

D ≈ 0.05 keV. Thus ν ≈ 200 in a typical R_d = 20 keV cascade. Closely spaced SI and vacancies quickly recombine and only about one-third of the initial displacements survive. Typically, this leaves a vacancy-rich cascade core, surrounded by a shell of SI (Figure 2c-e).

The majority of the SI quickly cluster to form small, disc-shaped features that are identical to small dislocation loops.[13] Along with SI, these loops are very mobile. Diffusion of SI and loops within the cascade region causes additional recombination prior to their rapid long-range migration (unless they are strongly trapped by other defects or solutes). Although they are less mobile than the SI, vacancies also eventually diffuse. Through a series of local jumps, the vacancies and solutes in the cascade quickly begin to evolve to lower energy configurations, forming small, three-dimensional clusters (Figure 2f), while others leave the cascade region.[12] The small clusters are unstable and can dissolve by vacancy emission. However, the small clusters also rapidly diffuse and coalesce with each other, forming larger nanovoids, which persist for much longer times. Solute atoms bind to the vacancies and segregate to clusters. The vacancy emission rate is lower from vacancy-solute cluster complexes. Small solute clusters remain after all the vacancy clusters have finally dissolved.

In summary, displacement cascades produce a range of sub-nm clusters (defects, solutes, and defect-solute complexes) that directly contribute to irradiation hardening. Expressing damage exposure, or neutron dose, in terms of displacements-per-atom (dpa) partially accounts for the effect of the neutron energy spectrum on the generation of cascade defects and the net residual defect production scales with dpa. For a typical RPV neutron spectrum, an end-of-life $\phi t_{>1} = 3 \times 10^{23}$ n/m² produces about 0.045±0.05 dpa. However, most of the vacancies and interstitials eventually migrate and annihilate at sinks long distances from the cascade region. Thus long-range diffusion results in additional nanostructural evolution.

Irradiation Induced Nanostructures

Current understanding of the evolution of embrittlement nanofeatures is based on combinations of sophisticated microstructural and microchemical characterization studies and physical models. Key characterization methods include: Small angle x-ray and neutron scattering,[6,14–16] various types of electron microscopy,[16,17] three-dimensional atom probe-field ion microscopy,[18] and positron annihilation spectroscopy.[19] Hardness recovery during annealing at T_a < 350°C has also been used to study features that have proven to be very difficult to characterize by other methods.[6] Thermodynamic-kinetic models are used to track the transport and fate of irradiation defects and solutes and to predict the number, size distribution and composition of the evolving nanofeatures.[6,8,20–22] While all of these tools have individual limitations, in combination they have provided considerable insight about the nanofeatures that can be divided into three broad categories:

- Copper rich or catalysed manganese-nickel rich precipitates (CRPs/MNPs).
- Unstable matrix defects (UMD) that form in cascades even in steels with low or no copper, but that anneal rapidly compared to typical low ϕ irradiation times.
- Stable matrix features (SMF) that persist or grow under irradiation even in steels with low or no copper

Most UMD are believed to be sub-nm vacancy clusters, complexed with solutes, that form in displacement cascades and dissolve in relatively short times (e.g., about 3 × 10⁵ sec at 290°C).[6] Hence, a large population of these features play a significant role in the magnitude and T_i and ϕ dependence of hardening only in the high ϕ regime, pertinent to accelerated test-reactor irradiation. While not, in themselves, important for surveillance or vessel ϕ << 10¹⁶ n/m²-s, some UMD serve as nucleation sites for larger SMF that are stabilized or grow due to a slight positive bias in the flow of SI to dislocations. (Most vacancies and SI annihilate in equal numbers at sinks.) Various solutes also segregate to nanovoids (and possibly loops) by long-range diffusion, contributing to the formation of SMF. Other possible SMF range from loose aggregates of solutes to nanoscale alloy (primarily molybdenum) carbo-phospho-nitro precipitates.[18]

An even more important consequence of displacement damage, however, is radiation-enhanced diffusion (RED) of solutes resulting from the excess concentration of vacancies. The primary consequence of RED is the formation of fine-scale CRPs.[6,8,9,14–16,20–22] The maximum effective concentration of supersaturated copper in the iron matrix is about 0.3%. This upper limit is imposed by coarse-scale copper pre-precipitation during the final stress relief treatment. The solubility is < 0.01% at around 290°C and, in the absence of irradiation, supersaturated copper slowly precipitates. However, radiation-enhanced diffusion enormously accelerates this process, resulting in the rapid formation of a high concentration (≥10²³ m³) of very small (~1.5–3 nm diameter) coherent (bcc) CRPs.

The CRPs are the dominant hardening feature in sensitive steels that have copper contents greater than about 0.05–0.1%, which is the minimum needed for rapid nucleation. The CRP ΔT_t contribution has a relatively weak T_i dependence and saturates at high ϕt, due to copper depletion from the matrix. At very high ϕ (>>10¹⁶ n/m²-s), the population of UMDs becomes significant, and acts as a vacancy-interstitial sink. This, in turn, reduces RED and delays the CRP evolution. At very low ϕ (<10¹⁴ n/m²-s), CRP evolution may be accelerated due to the contribution of thermal processes to copper diffusion. Recently, careful, single-variable test reactor studies have revealed a significant effect of dose rate in the intermediate ϕ regime.[23] This was not fully anticipated since an intermediate ϕ dose-rate effect had not been observed in previous analysis of the surveillance database.[4] Both temperature and alloy composition appear to play an important role in this ϕ-dependent regime, indicating a solute-vacancy trapping enhanced-recombination mechanism.

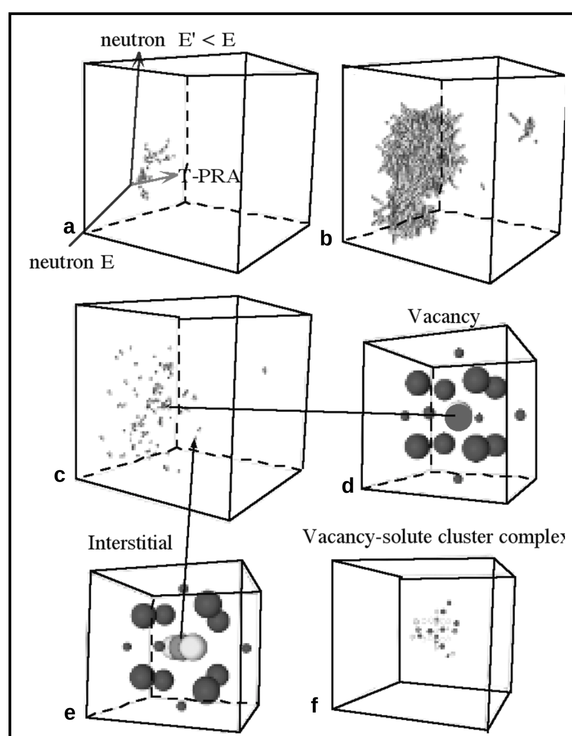

Figure 2. An illustration of cascade primary-damage production (iron atoms not shown in a–c and f): (a–c) MD simulation snapshots of initial intermediate and final dynamic stage of a displacement cascade; (d–e) vacancy and self interstitial defects; (f) vacancy-solute cluster complex formed after long-term cascade aging.

The CRPs are enriched in manganese and nickel, as well as smaller amounts of phosphorus and silicon.[6,8,20–22] The nickel and manganese strongly bind and amplify the effect of copper by increasing the volume of the precipitates. This explains the observation of a strong interaction between copper and nickel (and manganese) in increasing hardening and embrittlement. In some cases this can result in replacement of CRPs by manganese-nickel-rich precipitates (MNPs) with a small, copper-rich core. The MNPs are promoted by high manganese and nickel, low copper (beyond the amount needed for nucleation) and low T_i. Distinct MNPs have not been observed in RPV steels at very low copper levels, at least up to intermediate ϕt. However, the Cu-Mn-Ni-T_i regime for formation of MNPs at very high ϕt, if any, is not known. Recent proton irradiations of simple model steels with high nickel and manganese contents and no and low (0.05%) copper have shown significant hardening, suggesting the presence of MNPs.[24] The potential for the formation of such late-blooming phases in RPV steels under neutron irradiation is a major concern. Specifically, if nearly pure MNPs do eventually form, rapid embrittlement could occur even in low-copper steels.

Postirradiation annealing dissolves the SMF at about 375–400°C and the CRPs partially dissolve (losing most manganese and nickel and some copper) and coarsen at 425–450°C.[6,7] The smaller volume fraction and much lower number of nearly pure copper precipitates results in far less hardening. Hardening and embirttlement during subsequent re-irradiation is primarily due to the development of a new population of SMF. Residual copper in solution above about 0.07% may also precipitate as new CRPs. However, most of the copper may be effectively sequestered in the coarsened precipitates. Thus PIA at high T_a is an effective means of persistently reducing embrittlement.

TWO-FEATURE ENGINEERING MODELS OF IRRADIATION EMBRITTLEMENT AND ANNEALING

The physical understanding and detailed models described in the previous sections have provided the basis for developing quantitative engineering predictions of ΔT_t.[4,6,8,9,25] Recently, the detailed models were used to derive simpler, but physically-based, equations for $\Delta T_t = f(Cu, Ni, T_i, \phi t, T_a, t_a, \ldots)$ that were statistically fit to the surveillance and PIA databases by non-linear, least-square regression analysis.[4,7] Consistency with independent data from well-controlled, single-variable test reactor experiments and mechanistic understanding guided selection of the best physical model from among a large number of statistically equivalent possibilities.

A two-feature model (SMF and CRP) of the form

$$\Delta T_t = Af_{smf}(T_i, \phi t, P) + Bf_{crp}(Cu, Ni, \phi, \phi t)$$

provides an excellent fit to the large (609 ΔT_t points) U.S. power reactor surveillance database, with a standard error of ±13°C. Both the coefficients for the SMF (A) and CRP (B) differ between welds, plates, and forgings. Welds are the most sensitive product form and the forgings are the least sensitive. For example, taking copper = 0.15 and $\phi t = 3 \times 10^{23}$ and the other variables as given below, the total SMF/CRP contributions to ΔT_t are 85/60°C (weld); 77/49°C (plate); and 52/31°C (forging). The lower sensitivity of the forgings is partly due to their lower manganese content, which is ≈0.8% compared to ≈1.5% for plates and welds. The CRP contribution to ΔT_t is accelerated at $\phi < 10^{14}$ n/m^2.

Figure 3 illustrates the dependence of ΔT_t on some irradiation and metallurgical variables. Unless otherwise indicated, the default variables are: welds, T_i = 290°C, $\phi t = 10^{23}$ n/m^2, P = 0.01%, Cu = 0.3%, Ni = 0.8% and $\phi = 5 \times 10^{14}$ n/m^2. Several trends are notable. The CRP term saturates at high ϕt due to the depletion of matrix copper (Figure 3a). There is a very strong interaction between copper-nickel (Figure 3b). The threshold and the effective maximum copper are about 0.07% and 0.3% (Figure 3c) due to the

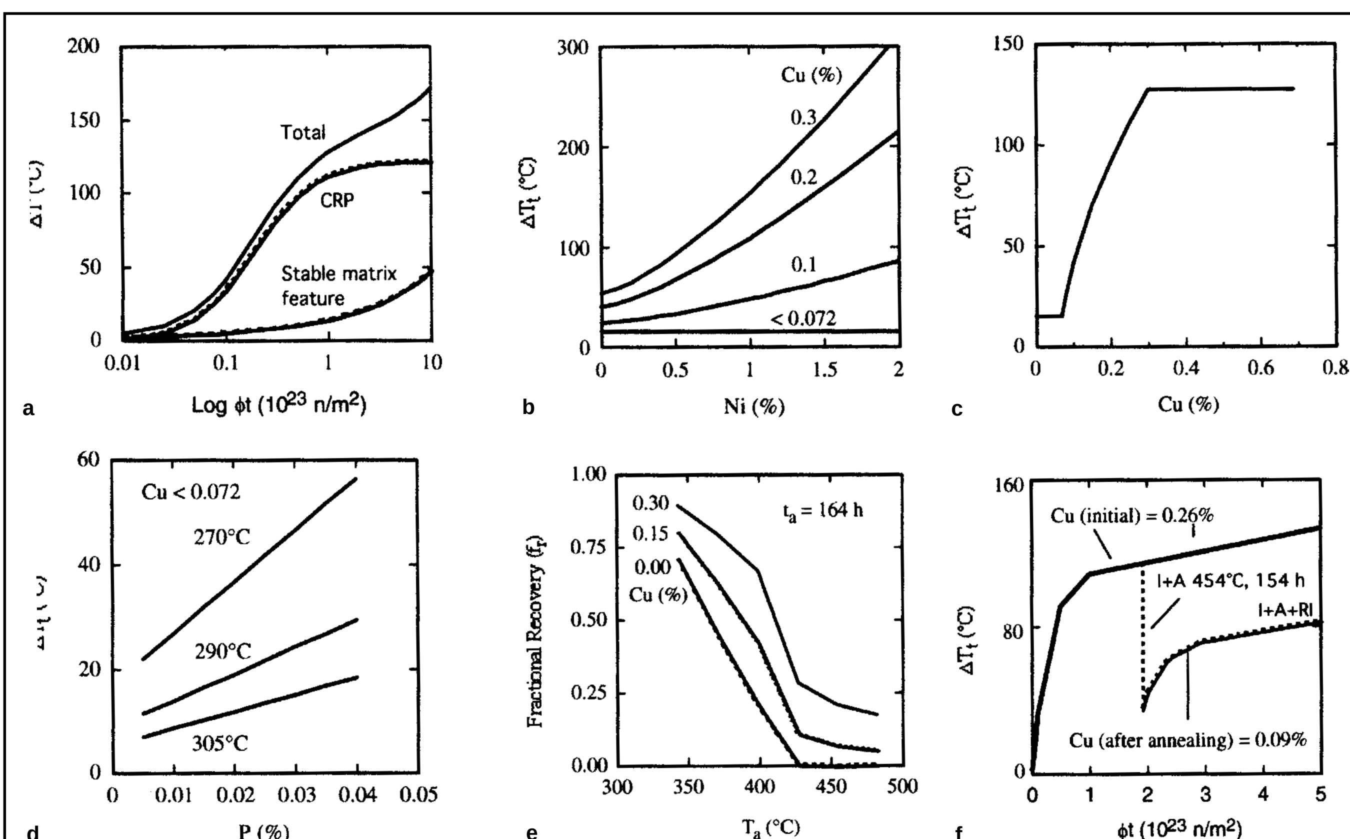

Figure 3. Physically-based statistical correlation model predictions of ΔT_t: (a) fluence dependence; (b) copper-nickel interaction dependence; (c) copper dependence; (d) T_i and P dependence of the SMF; (e) fractional PIA recovery; and (f) PIA and re-embrittlement.

CRP nucleation and pre-precipitation limits, respectively. While detailed refinements are possible, all of these trends in the CRP term are in excellent agreement with both independent experiments and the current understanding of embrittlement mechanisms.[6,8,20–22] The ΔT_t due to the SMF increases roughly with the square root of ϕt (Figure 3a) as well as with increasing P and decreasing T_i (Figure 3d). These trends are also consistent with independent sources of information. However, the causes, character, and consequences of the SMF are not as well understood as in the case of CRPs, and improved treatments of their contributions to ΔT_t (and the corresponding scatter) will require additional research.

The two-feature models have also been applied to correlating data to predict the residual shift (ΔT_{ta}) following PIA.[7] The fractional recovery ($f_r = \Delta T_{ta}/\Delta T_t$) primarily depends on T_a, t_a, T_i and Cu (Figure 3f). Below 400°C, f_r also depends on ϕ, due to a third hardening contribution of the UMD in the high ϕ test reactor data used in the analysis. Microhardness recovery data from both single-variable test reactor studies and surveillance specimens provided independent confirmation of the annealing-recovery model. The formulations for embrittlement and PIA can be combined to predict re-embrittlement, (ΔT_{tar}) assuming that high T_a returns the steel to its original state, except for the reduction of dissolved copper. For example, Figure 3g shows the predicted embrittlement for a 0.26% copper weld annealed at 454°C for 164 h, assuming that the residual copper is 0.09%. The re-embrittlement is moderate and PIA provides a persistent ΔT_{tar} advantage relative to the unannealed condition. The residual copper can be estimated from measurements or models and used as a basis to optimize the selection of T_a and t_4.

CONCLUSION

Despite progress in predicting irradiation embrittlement and recovery, a number of issues are not fully resolved or quantified. These include the role of product form; the effect of dose rate in the intermediate ϕ regime; the maximum effective copper content as a function of details of thermal processing history; the effects of secondary variables and variable combinations currently not, or only crudely, accounted for (e.g., manganese or phosphorus); the magnitude and scatter in the SMF contribution, particularly at high ϕt; through-wall attenuation; the potential for forming late-blooming phases in low-copper steels; thermal embrittlement or other new phenomena that might occur at long-times or very high ϕt, beyond the current database. Perhaps the most difficult issue is associated with material variability and the inherent uncertainties about the composition and properties of the steels in the RPV itself.

In addition to the resolution of these issues, the recently proposed master-curve method (ASTM E1921-97) provides a major opportunity to replace the current indirect and approximate CVN-based method for establishing irradiated toughness-temperature curves.[5] The master-curve method is based on the empirical observation of a universal mean toughness-reference temperature relation, $K_{mc}(T-T_o)$, that is physically superior to the current $K_{Ir}(T-T_{ndt})$ approach. The reference temperature (T_o), indexed at a reference toughness (100 MPa $\sqrt{m}$), can be measured with a relatively small number of relatively small fracture specimens. Further, the master-curve method uses Weibull-based statistical procedures to evaluate bounding toughness-temperature curves at specified confidence levels. Statistical considerations are also used to adjust measured toughness values to a common thickness (25.4 mm) to account for specimen size effects. Relatively permissive constraint limitations on specimen size and statistical procedures for censoring invalid data appear to allow the direct use of precracked Charpy bars. Techniques have been developed to permit the use of reconstituted broken Charpy specimens that could increase greatly the availability of steels from surveillance programs, thus enabling direct evaluation of irradiated toughness-temperature curves.

While the master-curve method represents a revolutionary advance in establishing fracture toughness in the cleavage transition, it rests on a series of empirically based assumptions and faces a number of challenges related to its application to assessing the integrity of irradiated pressure vessels. Issues regarding the key assumptions include the validity of a universal master-curve shape as well as both statistical and constraint-mediated size effects. Issues associated with the use of the master-curve method in integrity assessments include the applicability to dynamic and arrest toughness, effects of irradiation on the master-curve assumptions, ties to the Charpy-based surveillance database, effects of realistic surface/shallow flaw configurations, and the reliability of data from archival-surveillance materials to represent actual vessel steels. Resolving these issues and providing a robust physical basis for the MC is an important objective of future research.

ACKNOWLEDGEMENTS

The authors express their appreciation of the large number of people in the U.S. and around the world who have contributed to this work, with special thanks to Randy Nanstad, for many helpful discussions. Particular thanks go our former students, Brian Wirth and Erik Mader, and to our current student Howard Rathbun. The diligence and intellectual efforts of these individuals have contributed greatly to the improved understanding of the embrittlement and fracture mechanisms in RPV steels. We also thank our staff engineers Doug Klingensmith and David Gragg for their dedication to the UCSB RPV research effort. Finally, we gratefully acknowledge the support of the U.S. Nuclear Regulatory Ccommission for much of the research that is described in this article.

References

1. *Rules and Regulations Title 10 Code of Federal Regulations Part 50 Fracture Toughness Requirement* (Washington, D.C.: U.S. Government Printing Office, U.S. Nuclear Regulatory Commission, 1986).
2. *Boiler and Pressure Vessel Code Section III App. G Protection Against Nonductile Fracture* (New York: American Society of Mechanical Engineers, 1986).
3. *Regulatory Guide 1.99-Rev 2: Radiation Embrittlement to Reactor Pressure Vessel Materials* (Washington, D.C.: U.S. Government Printing Office, U.S. Nuclear Regulatory Commission, 1988).
4. E.D. Eason, J.E. Wright, and G.R. Odette, *Improved Embrittlement Correlations for Reactor Pressure Vessel Steels*, NUREG/CR-6551 (Washington, D.C.: U.S. Government Printing Office, U.S. Nuclear Regulatory Commission, 1998).
5. *Standard Test Method for Determination of Reference Temperature To for Ferritic Steels in the Transition Range*, ASTM E1921-97 Annual Book of ASTM Standards 03.01 (West Conshohocken, PA: ASTM, 1998), pp. 1068–1084.
6. G.R. Odette and G.E. Lucas, "Recent Progress in Understanding Reactor Pressure Vessel Embrittlement," *Rad. Effects and Defects in Solids*, 144 (1998), pp. 189–231.
7. E.D. Eason et al., "Embrittlement Recovery Due to Annealing of Reactor Pressure Vessel Steels," *Nucl Eng Des.*, 179 (3) (1998), pp. 257–265.
8. G.R. Odette et al., "Multiscale-Multiphysics Modeling of Radiation Damaged Materials: Embrittlement of Pressure Vessel Steels," *MRS Bulletin*, 26 (3) (2001), pp. 176–181.
9. G.R. Odette and G.E. Lucas, "Irradiation Embrittlement of Reactor Pressure Vessel Steels: Mechanisms, Models and Data Correlations," *Radiation Embrittlement of Reactor Pressure Vessel Steels—An International Review*, ASTM STP 909, ed. L.E. Steele (Philadelphia, PA: ASTM, 1986), pp. 206–241.
10. G.R. Odette, P.M. Lombrozo, R.A. Wullaert, "The Relationship Between Irradiation Hardening and Embrittlement of Pressure Vessel Steels," *Effects of Radiation on Materials—12th Int. Symp.*, ASTM STP 870, ed. F.A. Garner and J.S. Perrin (Philadelphia, PA: ASTM, 1985), pp. 840–860.
11. R.E. Stoller, G.R. Odette, and B.D. Wirth, "Primary Damage Formation in BCC Iron," *J. Nucl. Mater.*, 251 (1997), pp. 49–60.
12. B.D. Wirth and G.R. Odette, "Kinetic Lattice Monte Carlo Simulations of Cascade Aging in Dilute Iron-Copper Alloys," *Microstructural Processes in Irradiated Materials*, MRS Symp. Proc. 540, ed. J Zinkle et. al. (Warrendale, PA : MRS, 1999), pp. 637–642.
13. B.D. Wirth et al., "Dislocation Loop Structure Energy and Mobility of Self-interstitial Atom Clusters in BCC Iron," *J. Nucl. Mater.*, 276 (2000), pp. 33–40.
14. G.F. Solt et al., "Irradiation Induced Precipitation in Model Alloys with Systematic Variations of Cu, N and P Content: A Small Angle Neutron Scattering Study," *Effects of Radiation on Materials—16th Int. Symp.*, ASTM STP 1175, ed. A.S Kumar et al. (West Conshohocken, PA: ASTM, 1993), pp. 444–462.
15. W.J. Phythian and C.A. English, "Microstructural Evolution in Reactor Pressure-Vessel Steels," *J. Nucl. Mater.*, 205 (1993), pp. 162–177.
16. T.J. Williams and W.J. Phythian, "Electron Microscopy and Small Angle Neutron Scattering Study of Precipitates in Low-Alloy Submerged-Arc Welds," *Effects of Radiation on Materials—17th Int. Symp.*, ASTM 1270, ed. D.S. Gelles et al. (West Conshohocken, PA: ASTM, (1996), pp. 191–205.
17. M.L. Jenkins, "Characterization of Radiation Damage Microstructures by TEM," *J. Nucl. Mater.*, 216 (1994), pp. 125–156.
18. M.K. Miller, P. Pareige, and M.G. Burke, "Understanding Pressure Vessel Steels: An Atom Probe Perspective," *Materials Characterization* , 44 (2000), pp. 235–254.
19. B.D. Wirth et al., submitted to *Phys. Rev. B*.
20. G.R. Odette, "Radiation Induced Microstructural Evolution in Reactor Pressure Vessel Steels," *Microstructural Evolution During Irradiation*, MRS. Symp. Proc. 373, ed. I. Robertson et al. (Pittsburgh, PA: MRS, 1995), pp. 137–148.
21. G.R. Odette and B.D. Wirth, "A Computational Microscopy Study of Nanostructural Evolution in Irradiated Pressure Vessel Steels," *J. Nucl. Mater.*, 251 (1997), pp. 157–171.
22. D.L. Liu et al., "A Lattice Monte Carlo Simulation of Nanophase Compositions and Structures in Irradiated Pressure Vessel Fe-Cu-Ni-Mn-Si Steels," *Mater. Sci. Eng. A—Struct.*, 238 (1) (1997), pp. 202–209.
23. G.R. Odette, G.E. Lucas, and D. Klingensmith "On the Effects of Neutron Flux and Composition on Hardening of Reactor Pressure Vessel Steels and Model Alloys," *Microstructural Evolution During Irradiation*, MRS. Symp. Proc., ed. G.E. Lucas et al. (Pittsburgh, PA: MRS, 2001), in press.
24. Q. Yu et al., "Hardening and Microstructure of Model Reactor Pressure Vessel Steel Alloys Using Proton Irradiation," *Microstructural Evolution During Irradiation*, MRS. Symp. Proc., ed. G.E. Lucas et al. (Pittsburgh, PA: MRS, 2001), in press.
25. S.B. Fisher and J.T. Buswell, "A Model For PWR Pressure-Vessel Embrittlement," *Int. J. Pressure Vessels and Piping*, 27 (2) (1987), pp. 91–135.

G.R. Odette and G.E. Lucas are professors in the Department of Mechanical and Environmental Engineering at the University of California, Santa Barbara.

For more information, contact G.R. Odette, University of California at Santa Barbara, Department of Mechanical and Environmental Engineering, Santa Barbara, CA 93106; (805) 893-3525; fax (805) 893-8651; e-mail odette@engineering.ucsb.edu.